Analytical Design for Optimum Filamentary Pressure Vessels

HANS U SCHUERCH* AND ODUS R BURGGRAF†
Astro Research Corporation, Santa Barbara, Calif

An analytic treatment of the equilibrium configurations for thin-walled, axisymmetric, rotating, filamentary pressure vessels is presented Solutions in the form of tabulated elliptical integral functions are developed for the pertinent geometrical characteristics of the structural shapes and for their associated filamentary geometries A morphological review of the corresponding structures is presented, based upon a discussion of the mathematical properties of the solutions Experimental realization of the equilibrium configuration of various filamentary structures, including stationary pressure vessels and rotating single filaments, confirms the validity of the analytic expresions Applications of formulas to problems of external loadings and of the static stability of filamentary, pressure stabilized structures demonstrate the utility of the analytical technique A brief discussion of weight and engineering properties, including performance of optimum, isotensoid pressure vessels and related filamentary composite materials, is presented in the Appendix

Nomenclature

C	= $\sin\beta_0$
$E_{(\psi\ k)}\ E_{(k)}$	= elliptic integrals of the second kind
$F_{(\psi\ k)}, F_{(k)}$	= elliptic integrals of the first kind
F_{tub}	= tensile ultimate strength under biaxial stress
F_{tuu}	= tensile ultimate strength under uniaxial stress
H	= see Eq (17c)
J_n	= integral defined by Eq (20)
K	= $2\pi p_0 r_0^2/nT$, pressure parameter
k	= modulus of elliptic integral
l	= filament length
L	= l/r_0
m'	= filament mass per unit length
n	= number of windings
N	= force on filament
p	= pressure (p_0 = pressure at $r = r_0$)
r	= radius from axis of symmetry
r_0	= equatorial radius
R	= r/r_0
s	= F_{tu}/ρ, specific strength
T	= tension in filament
T_0	= tension at $r = r_0$
V	= volume
W	= weight
x	= R^2
x_2, x_3	= see Eqs (17)
y	= see Eq (16)
z	= distance along axis of symmetry
Z	= z/r_0
(PE)	= potential energy
(SE)	= strain energy
(SF)	= safety factor
(WR)	= weight ratio
α	= angle between tangent to meridian curve and z axis, also argument of elliptical integral of the third kind
β	= helix angle
ϵ	= strain
$\Lambda_{0(\psi\ k)}$	= Heuman lambda function, see Eq (27)
$\Pi_{(\psi\ \alpha^2\ k)}, \Pi_{(\alpha^2\ k)}$	= elliptic integrals of third kind
φ	= central angle
Ω	= $m'r_0^2\omega^2/T_0$, centrifugal loading parameter
ω	= angular velocity
ρ_f	= density of fluid
ρ, ρ_m	= density of solid
η	= design efficiency

Presented as Preprint 2914-63 at the AIAA Launch and Space Vehicle Shell Structures Conference, Palm Springs, Calif , April 1–3, 1963; revision received March 6 1964 The work presented in this paper has been conducted with the financial support of NASA

* President Associate Fellow Member AIAA
† Consultant Member AIAA

I Introduction

THE use of filamentary structures is of continually increasing interest for applications requiring ultimate structural performance Such performance is made possible by exploiting the remarkable physical properties of materials in the form of thin, continuous fibers In the case of pressure vessels, for instance, it can be shown that considerable improvements in structural performance are obtainable Moreover, considerable additional freedom in the choice of optimum design configurations is possible by employing filamentary materials rather than the more conventional sheet metals used in high-performance pressure vessel fabrication A discussion of some basic facts pertinent to this statement is presented in the Appendix

As a consequence of the technical applications for filamentary structures, a need has arisen for a workable engineering theory of thin shells made from anisotropic, filamentary composites Theories for stresses and deformations in such structures are based upon two basically different approaches: analysis from the point of view of reinforced, anisotropic shell theory or, alternatively, from considerations of individual filaments

With the first method, stresses in the matrix material are easily accommodated, thus allowing great generality A fundamental treatment of this type of problem is given by Green and Adkins[1] in a chapter on reinforced materials A similar treatment applied to orthotropic materials is given, for instance, by Harmon [2]

With the second method, the matrix material usually is assumed to be completely compliant, the tension in the filament being the dominant load carrying stress in the structure The filament analysis, though more restricted, is simpler to apply and more readily yields usable information Thus, the case of filament-wound structures, subject to pure pressure loading, has been analyzed in detail The resulting concept of monotropic membranes as structural elements, and their analytic treatment, has been presented by the authors in Ref 3 The special case of isotensoid structures representing an optimum design configuration due to the uniformity of filament stress has been discussed by Hoffman and Schuerch [4 5 12] and, for the special case of filament-wound pressure vessel end-closures, by Zickel,[6] Hartung[11] and Nourse, et al [13]

A conceptual error is evident in Refs 6, 11, and 13, related to the apparent nonreturn and "forbidden zone" characteristics of isotensoid end-domes This error is associated with the restrictions in the formulations to uniform internal pressure which prevents proper consideration of interface

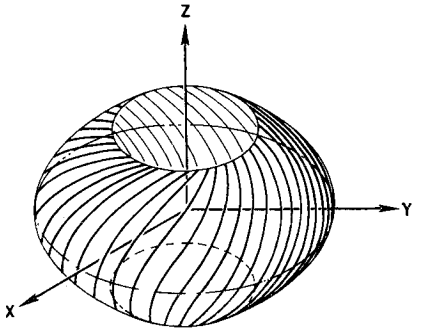

Fig 1 Monotropic membrane of revolution

pressure of the insert flange of filament wound end-domes (Ref 3, p 25, and Ref 12)

In many proposed applications of filamentary structures, centrifugal loading of the filaments is expected to be important The basic equilibrium conditions for combined pressure and centrifugal loading were given in Ref 3; however, in further analysis of the filament geometry, only pressure loading was considered The present paper is concerned with analyzing the effects of centrifugal loading on filament wound pressurized structures

In contrast to Ref 3, wherein numerical results were obtained by integrating the equilibrium equations on a digital computer, the present paper gives the results in the form of analytic expressions involving tabulated functions The results of Ref 3 may be obtained from these formulas as a special case As a further distinction, the basic differential equations for monotropic membranes were developed in Ref 3 from differential geometrical considerations of lines on surfaces without initial restriction to surfaces of revolution An alternate derivation of the equilibrium condition for the particularly interesting case of surfaces of revolution is given here for the sake of completeness

II Basic Differential Equations

A Equilibrium Conditions

Consider a uniformly spaced array of n filaments placed on a surface of revolution as shown in Fig 1 If the spacing is small, the filaments will constitute a structure that can be described as a monotropic membrane [3] Assume this structure to be subject to loads generated by an internal positive pressure p and by rotation with angular velocity ω around the z axis Assume further that a nonstructural liner contains the internal pressure and distributes the pressure loads equally among the filaments without further contribution to the load carrying function of the structure

Now consider an individual filament as a completely flexible but axially stiff structural element To determine filament shape, apply three independent equilibrium conditions: 1) equilibrium of torques about the z axis; 2) equilibrium of forces in the z direction; and 3) equilibrium of forces parallel to the filament To apply these equilibrium conditions, the corresponding force components are needed Referring to Fig 2 for notation, the components of the tension in the filament are simply

$$T\varphi = T \sin\beta \tag{1a}$$

$$T = T \cos\beta \cos\alpha \tag{1b}$$

$$T = T \cos\beta \sin\alpha \tag{1c}$$

The pressure force affects only the equilibrium of forces in the z direction The angular separation between adjacent filaments is $2\pi/n$, where n is the number of filaments crossing the plane $z = 0$ Hence, the distance separating the filaments at radius r is just $2\pi r/n$, and the z components of the pressure force on a filament per differential increment of radius are given by

$$dN = 2\pi pr\, dr/n \tag{2}$$

The centrifugal force affects only the equilibrium condition along the axis of the filament, so that only the component parallel to the filament is needed The centrifugal force for a length dl of filament of linear density m' is $dN = m'r\omega^2 dl$, where ω is the angular velocity of the filament about the z axis This radial vector resolves parallel to the filament to give

$$dN_T = (m'r\omega^2 dl) \sin\alpha \cos\beta$$

Since the element of length dl resolves along the radius vector according to $dl \sin\alpha \cos\beta = -dr$, the component of centrifugal force parallel to the filament is given by

$$dN_T = -m'r\omega^2 dr \tag{3}$$

With these expressions for the force components, the equilibrium conditions are now readily obtained. Since only the tension in the filament produces a torque about the z axis, equilibrium in torque requires that $rT\varphi$ be constant along the filament, or

$$Tr \sin\beta = T_0 r_0 \sin\beta_0 \tag{4}$$

where the constant has been evaluated at $z = 0$ ‡ For equilibrium of forces in the z direction, only the filament tension and pressure force contribute Hence, from Eqs (1b) and (2),

$$(d/dr)(T \cos\beta \cos\alpha) = 2\pi pr/n \tag{5}$$

The final condition of equilibrium of forces parallel to the filament involves only filament tension and centrifugal force From Eq (3) there results

$$dT/dr = -m'r\omega^2 \tag{6}$$

B Filament Orientation

Equation (6) may be integrated immediately to give

$$(T/T_0) = 1 + (\Omega/2)[1 - (r^2/r_0^2)] \tag{7}$$

where $\Omega = m'r_0^2\omega^2/T_0$

The constant of integration was evaluated at $z = 0$ Introducing nondimensional coordinates $R = r/r_0$ and $Z = z/r_0$ and the abbreviated notation $C = \sin\beta_0$, the azimuth angle β of the filament on its surface of revolution obtained from Eq (4) becomes

$$\sin\beta = \frac{C}{R[1 + \frac{1}{2}\Omega(1 - R^2)]} \tag{8}$$

Finally, the integral of Eq (5) is expressed as

$$T \cos\beta \cos\alpha = T_0 \cos\beta_0 + \frac{2\pi}{n}\int_r^{r_0} pr\,dr \tag{9}$$

(Note that $\alpha_0 = 0$ since $z = 0$ is taken as the plane of symmetry) If the pressurizing fluid has density ρ_f, then the steady-state pressure distribution is that for solid body rotation

$$p = p_0 + \tfrac{1}{2}\rho_f r^2\omega^2 \tag{10}$$

where p_0 is the pressure on the axis of rotation With this result, the integral in Eq (9) may be evaluated Thus, with $K = 2\pi p_0 r_0/nT_0$, Eq (9) reduces to

$$\left(\frac{T}{T_0}\right)\cos\beta \cos\alpha = \cos\beta_0 - \frac{1}{2}K(1 - R^2) \times \left[1 + \frac{1}{4}\frac{\rho_f\omega^2 r_0^2}{p_0}(1 + R^2)\right] \tag{11}$$

‡ For isotensoids (T = const), Eq (4) was obtained in Ref 3 from consideration of geodesic curves on a surface of revolution

Using Eqs (7) and (8), T and β may be eliminated:

$$\cos\alpha = \frac{(1 - C^2)^{1/2} - \frac{1}{2}K(1 - R^2)\,[1 + \frac{1}{4}(\rho_f\omega^2 r_0^2/p_0)(1 + R^2)]}{\{[1 + \frac{1}{2}\Omega(1 - R^2)]^2 - (C^2/R^2)\}^{1/2}} \tag{12}$$

C Filament Geometry

Although the orientation of the filament is determined completely by Eqs (8) and (12), its location in space is yet to be determined The angle denoted in Fig 2 may be defined by the relations

$$\frac{dZ}{dR} = -\cot\alpha = \pm\frac{\cos\alpha}{(1 - \cos^2\alpha)^{1/2}} \tag{13a}$$

$$R\frac{d\varphi}{dR} = -\frac{\tan\beta}{\sin\alpha} = \pm\frac{\sin\beta}{[1 - \sin^2\beta)(1 - \cos^2\alpha)]^{1/2}} \tag{13b}$$

Thus, from Eqs (8, 12, and 13a), the meridian curve must satisfy

$$\frac{dZ}{dR} = \pm\frac{(1 - C^2)^{1/2} - \frac{1}{2}K(1 - R)^2\,[1 + \frac{1}{4}(\rho_f\omega^2 r_0^2/p_0)(1 + R^2)]}{\{[1 + \frac{1}{2}\Omega(1 - R^2)]^2 - (C^2/R^2) - \{(1 - C^2)^{1/2} - \frac{1}{2}K(1 - R^2) \times [1 + \frac{1}{4}(\rho_f\omega^2 r_0^2/p_0)(1 + R^2)]\}^2\}^{1/2}} \tag{14}$$

Similarly, from Eqs (8, 12, and 13b), the central angle φ must satisfy

$$\frac{d\varphi}{dR} = \pm\frac{C/R^2}{\{[1 + \frac{1}{2}\Omega(1 - R^2)]^2 - (C^2/R^2) - \{(1 - C^2)^{1/2} - \frac{1}{2}K(1 - R^2)\,[1 + (\rho_f\omega^2 r_0^2/p_0)(1 + R^2)]\}^2\}^{1/2}} \tag{15}$$

The differential equations (14) and (15) completely determine the filament curves in space The radicand in the denominators is a fifth-degree polynomial in R^2 Hence, the integrals for $Z_{(R^2)}$ and $\varphi_{(R^2)}$ are hyperelliptic integrals of class 2; evaluation of such integrals usually requires either numerical integration or complicated series expansion However, closed form solutions in terms of tabulated functions may be obtained if the parameter $(\rho_f\omega^2 r_0^2/p_0)$ is set equal to zero, corresponding to a structure pressurized by a light fluid (or gas) The effect of centrifugal force then affects the filament geometry only through the parameter Ω With this simplification, the radicand in the denominators becomes a cubic in R^2, and the integrals reduce to ordinary elliptic integrals In the following, only the case $(\rho_f\omega^2 r_0^2/p_0 = 0)$ will be considered

III Integration of Equations

A The Factored Cubic

The differential equations for the meridian curve and the central angle both contain as a denominator the quantity

$$y = [(K^2 - \Omega^2)x^3 - 4\{\Omega[1 + (\Omega/2)] + K[(1 - C^2)^{1/2} - (K/2)]\}x^2 + 4\{(1 + \Omega/2)^2 - [(1 - C^2)^{1/2} - (K/2)]^2\}x - 4C^2]^{1/2} \tag{16}$$

where $x = R^2$, and where $(\rho_f\omega^2 r_0^2/p_0)$ has been set equal to zero To facilitate integration of the equations, the factored form of the radicand is preferred One root of the cubic radicand is $x_1 = 1$, corresponding to the previous choice of $z = 0$ as plane of symmetry Dividing out this root from the radicand leaves the quadratic

$$(K^2 - \Omega^2)x^2 + 4[K(1 - C^2)^{1/2} + \Omega - \tfrac{1}{4}(K^2 - \Omega^2)]x - 4C^2$$

The remaining two roots of the cubic are

$$x_2 = -\frac{2}{K^2 - \Omega^2}\{H - [H^2 + C^2(K^2 - \Omega^2)]^{1/2}\} \tag{17a}$$

$$x_3 = -\frac{2}{K^2 - \Omega^2}\{H + [H^2 + C^2(K^2 - \Omega^2)]^{1/2}\} \tag{17b}$$

where

$$H = K(1 - C^2)^{1/2} + \Omega - \tfrac{1}{4}(K^2 - \Omega^2) \tag{17c}$$

Thus, in factored form,

$$y = [(K^2 - \Omega^2)(1 - x)(x - x_2)(x - x_3)]^{1/2} \tag{18}$$

The particular ordering of the roots indicated in Eq (18) is not the only possible choice Altogether, there are 24 permutations of the inequality $x_3 < x_2 < x < 1$ providing positive values of the radicand (12 for $K > \Omega$ and 12 for $K < \Omega$) However, most of these permutations do not correspond to physically realizable values of Ω, K, and C for rotating, pressurized structures A critical examination of Eqs (17) for the roots x_2 and x_3 reveals the following theorems, which determine the acceptability of a given permutation of the roots:

Theorem A: for $K > \Omega$, $x_2 \geq 0$, and $x_3 \leq 0$ for all physically realizable values of K, Ω, and C

Theorem B: for $K < \Omega$, $x_2 \geq 0$, $x_3 > x_2$, and also $x_3 > 1$ for all physically realizable values of K, Ω, and C

In addition, the initial condition $Z = 0$ at $x = 1$ provides the condition that x and 1cannot be separated by x_2 or x_3

Application of these criteria shows that the only physically realizable orderings of the roots are the following:

Case A

$$K > \Omega,\ x_3 < x_2 < x < 1 \tag{19a}$$

Case B

$$K > \Omega,\ x_3 < 1 < x < x_2 \tag{19b}$$

Case C

$$K < \Omega,\ x_2 < x < 1 < x_3 \tag{19c}$$

Case D

$$K < \Omega,\ 1 < x < x_2 < x_3 \tag{19d}$$

A discussion of the physical significance of these distinct cases is deferred until the section on morphology of the structures For the present, it is merely noted that the analytical form of the solution may be different for each of these four cases

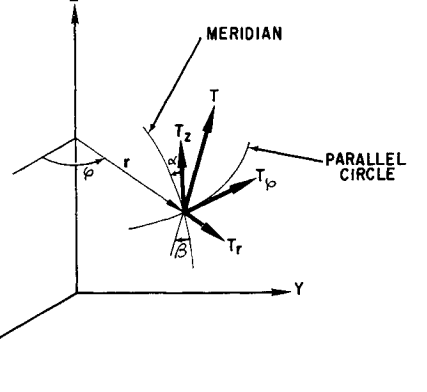

Fig 2 Coordinates and notations

B Meridian Curve

From the condition of axial symmetry, the filaments form a surface that may be considered to be generated by rotating a curve in a meridian plane (φ = const) around the z axis The slope of this meridian curve is given by Eq (14), which reduces to ($\rho_f = 0$):

$$\frac{dZ}{dx} = \pm \frac{\frac{1}{2}\{[(1-C^2)^{1/2} - (K/2)] + (K/2)x\}}{\{x[1 + \frac{1}{2}\Omega(1-x)]^2 - C^2 - [(1-C^2)^{1/2} - (K/2)(1-x)]^2\}^{1/2}}$$

With y defined by Eq (16), introduce the notation

$$J_{n(x)} = \int_x^1 \frac{x^n dx}{y} \tag{20}$$

The meridian curve is given in terms of the J integrals:

$$Z_{(x)} = \pm\{[(K/2) - (1-C^2)^{1/2}]J_{0(x)} - (K/2)J_{1(x)}\}$$

For cases A and D, the meridian curves are given by

$$Z_{(x)} = \pm \frac{1}{[(K^2 - \Omega^2)(1-x_3)]^{1/2}} \{[K(1-x_3) - 2(1-C^2)^{1/2}]F(\psi,k_1) - K(1-x_3)E(\psi_1,k)\} \tag{21}$$

where

$$\sin\psi_1 = \left(\frac{1-x}{1-x_2}\right)^{1/2} \qquad k_1 = \left(\frac{1-x_2}{1-x_3}\right)^{1/2}$$

For the other two cases, the modulus k becomes imaginary Hence, for cases B and C, the alternate form of the integrals is used:

$$Z_{(x)} = \pm \frac{1}{[(K^2 - \Omega^2)(x_2 - x_3)]^{1/2}} \times \{-[K(1-x_3) - 2(1-C^2)^{1/2}] \times [F(k_2) - F(\psi_2,k_2)] + K(x_2 - x_3)[E(k_2) - E(\psi_2,k_2)]\} \tag{22}$$

where

$$\sin\psi_2 = \left(\frac{x_2 - x}{x_2 - 1}\right)^{1/2} \qquad k_2 = \left(\frac{x_2 - 1}{x_2 - x_3}\right)^{1/2}$$

An exceptional case remains for consideration: $K = \Omega$ By considering the limiting behavior of Eqs (17), the roots of the cubic are found to go as

$$\lim_{K\to\Omega} x_2 = \frac{C^2}{\Omega[1 + (1-C^2)^{1/2}]} \tag{23a}$$

$$\lim_{K\to\Omega} x_3 = \pm\infty \tag{23b}$$

Consider the form of solution given by Eq (21); then

$$\lim_{K\to\Omega} [(K^2 - \Omega^2)(1-x_3)]^{1/2} = 2\{\Omega[1 + (1-C^2)^{1/2}]\}^{1/2}$$

and

$$\lim_{K\to\Omega} k_1 = 0$$

With the series expansions of the elliptic integrals

$$F(\psi,k) = \int_0^\psi \frac{d\psi}{(1 - k^2\sin^{-2}\psi)^{1/2}} = \psi + \frac{1}{4}k^2(\psi - \sin\psi\cos\psi) +$$

$$E(\psi,k) = \int_0^\psi (1 - k^2\sin^2\psi d\psi)^{1/2} = \psi - \frac{1}{4}k^2(\psi - \sin\psi\cos\psi) +$$

and with the forementioned limiting values, the solution for $K = \Omega$ is found to be

$$Z = \pm \frac{1}{\{\Omega[1 + (1-C^2)^{1/2}]\}^{1/2}} \left\{\left[\frac{\Omega}{4}(1-x_2) - (1-C^2)^{1/2}\right] \arcsin\left(\frac{1-x}{1-x_2}\right)^{1/2} - \frac{\Omega}{4}[1-x)(x-x_2)]^{1/2}\right\} \tag{24}$$

where x_2 is given by Eqs (23) For $C = 0$ (meridian-wrapped filaments), Eq (24) reduces to

$$Z = \{[1/(2\Omega)^{1/2}](1 - \tfrac{1}{4}\Omega)\arcsin(1-x)^{1/2} + \tfrac{1}{8}[2\Omega x(1-x)]^{1/2}\} \tag{25}$$

Equation (24) has been verified as the integral of Eq (14) for $K = \Omega$ (with $\rho_f = 0$) by direct differentiation

Finally, the condition for the meridian curve of a cusp needs to be considered

Denote by x_0 the value of x for zero slope, and recall that x_2 is the value of x for infinite slope Then the cusp condition is $x_0 = x_2$ From Eq (14) (with $\rho_f = 0$),

$$x_0 = 1 - (2/K)(1-C^2)^{1/2}$$

while x_2 is given by Eq (17) Hence the condition $x_0 = x_2$ is given by

$$\left\{\frac{\Omega^2 - K^2}{2}\left[1 - \frac{2}{K}(1-C^2)^{1/2}\right] - H\right\}^2 = H^2 - C^2(\Omega^2 - K^2)$$

Squaring, collecting terms, and dividing out $(\Omega^2 - K^2)$, we are left with the expression

$$K^2(1-\Omega) + \Omega^2(1-C^2) - (K^2 + \Omega^2 - 4\Omega)(K/2)(1-C^2)^{1/2} = 0$$

which is a quadratic in either Ω or $1 - C^2$ As a quadratic in Ω, we have

$$\Omega^2[(K/2)(1-C^2)^{1/2}x_0] + \Omega K^2 x_0 - (K^4/4)[(4/K^2) - 1 + x_0] = 0$$

By the quadratic formula,

$$\Omega = -\frac{K}{(1-C^2)^{1/2}}\left\{1 \pm \left[1 + \frac{2(1-C^2)}{K}\left(\frac{1 - (K/2)(1-C^2)^{1/2}}{1 - (2/K)(1-C^2)^{1/2}}\right)\right]^{1/2}\right\}$$

To have $\Omega > 0$, we take the lower sign Rewriting the radicand we obtain finally

$$\Omega = \frac{K}{(1-C^2)^{1/2}}\left\{\left[\frac{C^2}{1 - (2/K)(1-C^2)^{1/2}}\right]^{1/2} - 1\right\}$$

In terms of x_0,

$$\Omega = \frac{2}{1-x_0}\left\{\left(\frac{C^2}{x_0}\right)^{1/2} - 1\right\} \qquad K = \frac{2(1-C^2)^{1/2}}{1-x_0}$$

C Central Angle

If the parameter C is not zero, the filament will advance around the z axis as it is wound The central angle φ (see Fig 2) is determined by integrating Eq (15) In terms of

the variable $x = R^2$, and for $\rho_f = 0$, this equation reduces to

$$\frac{d\varphi}{dx} = \pm \frac{C/2}{x\{x[1 + \frac{1}{2}\Omega(1-x)]^2 - C^2 - x[(1-C^2)^{1/2} - \frac{1}{2}K(1-x)]^2\}^{1/2}}$$

In terms of the J integrals defined by Eq (20), the central angle is given by

$$\varphi = \pm C \int_x^1 \frac{dx}{xy} = \pm C J_{-1}(x) \tag{26}$$

The integral J_{-1} involves the incomplete elliptic integral of the third kind which in turn involves theta functions These functions are tabulated in Ref 9 or, alternatively, can be evaluated by means of an infinite series The complete integral may be evaluated in terms of Heuman's lambda function Λ_0, which is tabulated in Ref 7, for example Λ_0 is given in terms of the elliptic integrals of first and second kinds by

$$(\pi/2)\Lambda_0(\psi,k) = [E(k) - F(k)]F(\psi,k^1) + F(k)E(\psi,k^1) \tag{27}$$

where $k^1 = (1 - k^2)^{1/2}$ Thus, for case A [Eq (19a)], we obtain

$$\varphi_{(x_2)} = \pm \frac{\pi C}{[-x_2 x_3 (K^2 - \Omega^2)]^{1/2}} \Lambda_0(\xi_1,k_1) \tag{28a}$$

where

$$\sin\xi_1 = \left(\frac{-x_3}{x_2 - x_3}\right)^{1/2} \qquad k_1 = \left(\frac{1 - x_2}{1 - x_3}\right)^{1/2}$$

For case B,

$$\varphi_{(x_2)} = \mp \frac{\pi C}{[-x_2 x_3 (K^2 - \Omega^2)]^{1/2}} \Lambda_0(\xi_2,k_2) \tag{28b}$$

where

$$\sin\xi_2 = \left(\frac{-x_3}{1 - x_3}\right)^{1/2} \qquad k_2 = \left(\frac{x_2 - 1}{x_2 - x_3}\right)^{1/2}$$

For case C,

$$\varphi_{(x_2)} = \mp \frac{C}{(\Omega^2 - K^2)^{1/2}} \left\{ \frac{2F(k_2)}{x_3(x_3 - x_2)^{1/2}} + \frac{\pi}{(x_2 x_3)^{1/2}} \Lambda_0(\eta_2,k_2) \right\} \tag{28c}$$

where

$$\sin\eta_2 = \left(\frac{x_3 - x_2}{x_3}\right)^{1/2} \qquad k_2 = \left(\frac{1 - x_2}{x_3 - x_2}\right)^{1/2}$$

For case D,

$$\varphi_{(x_2)} = \pm \frac{C}{(\Omega^2 - K^2)^{1/2}} \left\{ \frac{2F(k_1)}{x_3(x_3 - 1)^{1/2}} + \frac{\pi}{(x_2 x_3)^{1/2}} \Lambda_0(\eta_1,k_1) \right\} \tag{28d}$$

where

$$\sin\eta_1 = \left(\frac{x_3 - 1}{x_3}\right)^{1/2} \qquad k_1 = \left(\frac{x_2 - 1}{x_3 - 1}\right)^{1/2}$$

For the exceptional case $K = \Omega$, the incomplete integral may be evaluated in simple terms Consider the central angle for case A Since $k_1 \to 0$ in the limit as $K \to \Omega$, we find

$$\Pi(\psi_1,\alpha_1^2,0) = \int_0^{\psi_1} \frac{d\psi}{1 - \alpha_1^2 \sin^2\psi} = \frac{1}{(1 - \alpha_1^2)^{1/2}} \arctan[(1 - \alpha_1^2)^{1/2} \tan\psi_1]$$

where $\pi(\psi,\alpha,^2,0)$ is the elliptical integral of the third kind

Substituting the limiting formulas [given in Eqs (23) and following] into Eq (26), the central angle is obtained as

$$\tan\varphi = C \left[\frac{1 - x}{\{\Omega[1 + (1 - C^2)^{1/2}]x - C^2\}} \right]^{1/2} \tag{29}$$

This formula evidently applies for all four cases of Eqs (19) in the limit $K = \Omega$ By letting $x \to x_2$ in Eq (29), we observe that $\varphi \to \pi/2$; that is, in passing from outer radius to inner radius, the filament is wound a quarter turn about the z axis for the case $K = \Omega$ and for any $C \neq 0$

D Filament Length

The space curve generated by a filament is completely determined by $Z_{(R)}$ and $\varphi_{(R)}$ However, for many purposes, the filament length is needed also For example, to determine how a given filament-wound structure will deform under various combinations of pressure and centrifugal loading, the filament length and advance angle (central angle φ per turn) must be held invariant An expression for filament length is easily derived

From Fig 2, the differential element of length dL (normalized with respect to equatorial radius r_0) is given by $dL \cos\beta \cos\alpha = dZ$ Then, from Eqs (8, 12, and 14), with $\rho_f = 0$,

$$\frac{dL}{dx} = \pm \frac{(1 + \frac{1}{2}\Omega) - \frac{1}{2}\Omega x}{y} \tag{30}$$

where y is given by Eq (16) In terms of J integrals,

$$L = \pm[(1 + \tfrac{1}{2}\Omega)J_0 - \tfrac{1}{2}\Omega J_1] \tag{31}$$

Hence, for cases A and D of Eqs (19), substituting for J_0 and J_1, the filament length is given by

$$L = \pm \frac{1}{[(K^2 - \Omega^2)(1 - x_3)]^{1/2}} \{2F(\psi_1,k_1) + \Omega(1 - x_3)[F(\psi_1,k_1) - E(\psi_1,k_1)]\} \tag{32}$$

where

$$\sin\psi_1 = \left(\frac{1 - x}{1 - x_2}\right)^{1/2} \qquad k_1 = \left(\frac{1 - x_2}{1 - x_3}\right)^{1/2}$$

For cases B and C of Eqs (19), the alternate form of J_0 and J_1 should be used, resulting in the formula

$$L = \pm \frac{1}{[(K^2 - \Omega^2)(x_2 - x_3)]^{1/2}} \times \{[2 + \Omega(1 - x_3)]F(\psi_2,k_2) - \Omega(x_2 - x_3)E(\psi_2,k_2)\} \tag{33}$$

where

$$\sin\psi_2 = \left(\frac{x_2 - x}{x_2 - 1}\right)^{1/2} \qquad k_2 = \left(\frac{x_2 - 1}{x_2 - x_3}\right)^{1/2}$$

The exceptional case $K = \Omega$ may be evaluated as a limiting process as previously demonstrated for Eq (24) for the meridian curve and Eq (29) for the central angle Thus, in the limit as $K \to \Omega$, Eq (32) takes the form

$$L = \frac{\pm 1}{\{\Omega[1 + (1 - C^2)^{1/2}]\}^{1/2}} \{[1 + \tfrac{1}{4}\Omega(1 - x_2)] \times \arcsin\left(\frac{1 - x}{1 - x_2}\right)^{1/2} - \tfrac{1}{4}\Omega(1 - x)(x - x_2)\} \tag{34}$$

with x_2 given by Eq (23)

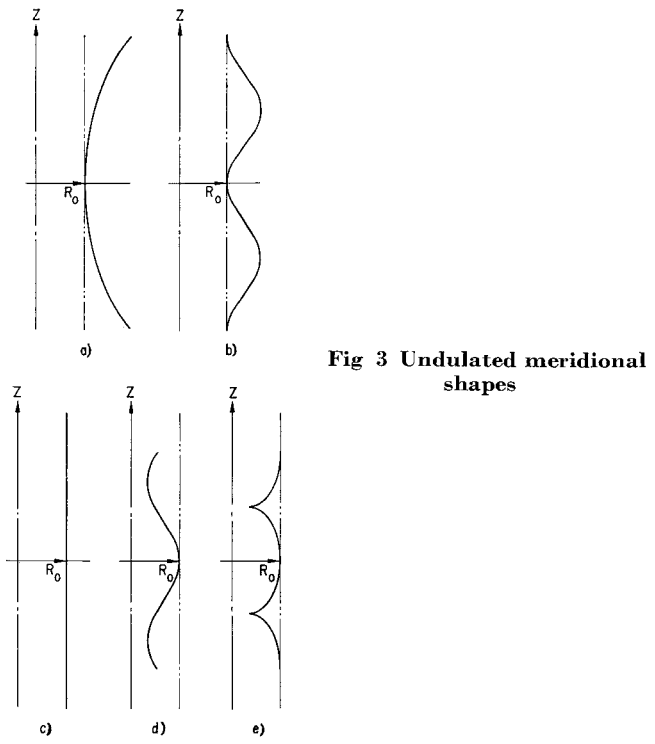

Fig 3 Undulated meridional shapes

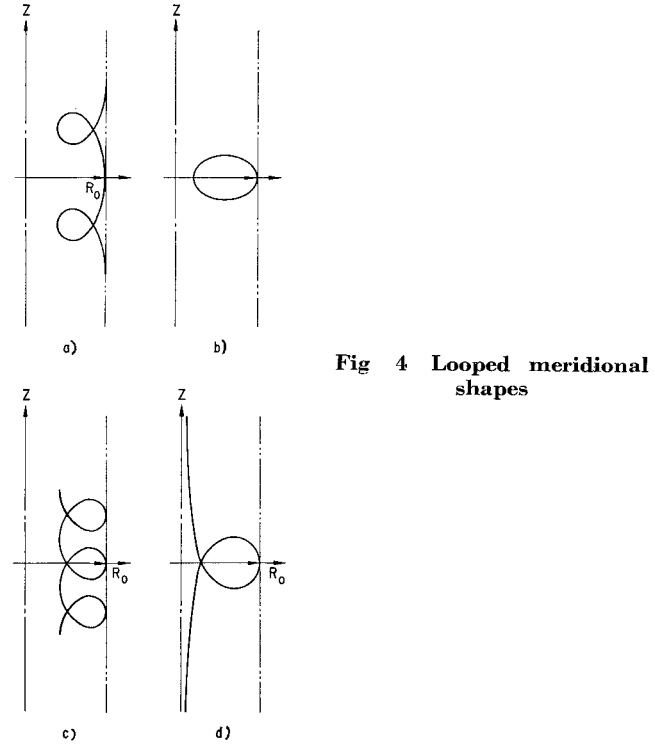

Fig 4 Looped meridional shapes

IV Discussion of Results

A Classification of Meridional Shapes

A morphology of axisymmetric filament-wound structures can be developed by discussing the range of possible solutions for the meridian given in Eq (21), (22), or (24) These equations show the meridional shape to depend on the three characteristic parameters K, Ω, and C, which define the pressure load intensity, the centrifugal load intensity, and the angularity of the winding pattern, respectively

For the purpose of this discussion, it will be assumed that both K and Ω are positive (or zero), corresponding to positive internal pressure and to tensile rather than compressive forces acting in the filaments The range of possible solutions, then, can be grouped into two classes of periodic functions according to their topological characteristics The two classes can be described as "undulating" (Fig 3) and "looped" (Fig 4) The corresponding surfaces of revolution are of the nature of corrugated tubes and toroids, respectively

The two classes of meridional curves are separated by the transitional case of a cusped function (Fig 3e) and bounded by a degenerate periodic function, which, in the case of the undulating species, assumes the shape of a hyperbola (Fig 3a); in the case of the looped species, it assumes the shape of a single loop with asymptotic branches (Fig 4d)

Each class can be further grouped into two types The undulating class may be "waisted" such that the reference radius r_0 is a minimum and $R \geq 1$ (Fig 3b); or it may be "bellied" such that the reference radius is a maximum and $R \leq 1$ (Fig 3c) The transitional case for the two types is the straight line $R \equiv 1$, corresponding to the meridian of a right circular cylinder (Fig 3c) The looped class may be "progressive" (Fig 4a), such that subsequent ordinates of $R = 1$ follow at values of increasingly larger positive Z if the curve is started at the coordinate $R = 1, Z = 0$ and followed in a direction of initially increasing Z; or it may be "regressive" (Fig 4c) in the sense that subsequent ordinates of $R = 1$ follow at increasingly negative Z The transitional case for these two types is the closed loop forming the meridian of a smooth toroid (Fig 4b)

A summary of the possible meridional forms is given in Table 1

A discussion of the transition cases is useful in defining the domains of existence of the various types in the $K - C - \Omega$ space By studying these singular types, the ranges of K, Ω, and C corresponding to the various classes of meridian curves may be established

Hyperboloid The hyperboloid corresponds to tension infinitely greater than the pressure or centrifugal force Hence the hyperboloid requires $K = 0, \Omega = 0$

Cylinder: The cylinder is defined by constant radius which requires $x_2 = 1$ This condition results in

$$\Omega = C^2 - K(1 - C^2)^{1/2} \tag{35}$$

Evidently, for cylinders, Ω cannot exceed unity for nonnegative K

Cusp The cusp divides the corrugated tubes from the progressive loops and requires the point of zero slope ($x = x_0$) to coincide with the point of infinite slope ($x = x_2$) This condition results in

$$\Omega = \frac{K}{(1 - C^2)^{1/2}} \left\{ \frac{C^2}{1 - (2/K)(1 - C^2)^{1/2}} - 1 \right\} \tag{36}$$

Cusps occur for all values of Ω; in the limit $\Omega \to \infty$, Eq (36) reduces to

$$K = 2\,(1 - C^2)^{1/2}$$

The limit $\Omega \to \infty$ may be viewed as the limit $T_0 \to 0$ and $p_0 \to 0$ such that K remains constant Then the radius of curva-

Table 1 Morphology of axisymmetric filament wound shells

Class	Undulating			Looped	
Type	Waisted	Bellied		Progressive	Regressive
Limiting and transition case	Hyperboloid	Cylinder	Cusp	Toroid	Asymptotic loop

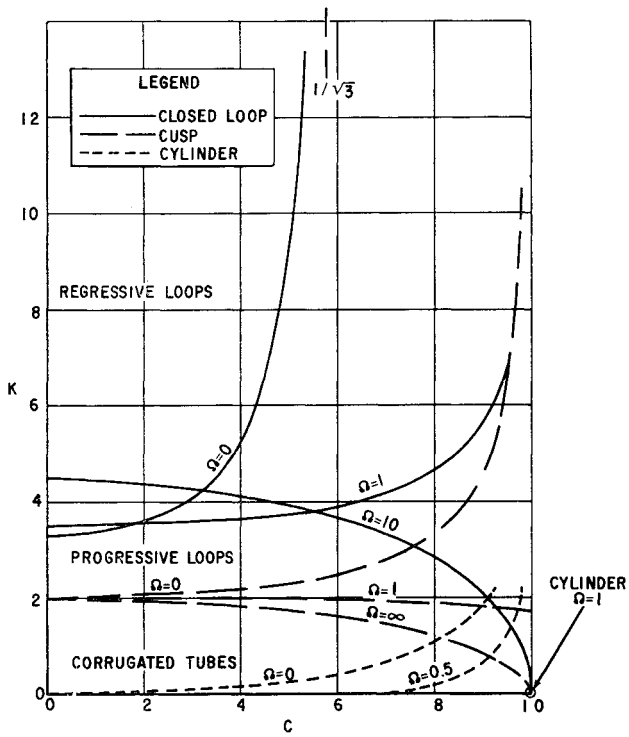

Fig 5 Domains for various classes of meridian curves

tube is zero at $x = 1$, and the filament lies along the radius

Toroid: The closed loop divides the progressive loops from the regressive loops and is defined by the condition $Z_{(x_2)} = 0$, where Z is given by Eqs (21) and (22) These equations are transcendental and an iterative technique must be used to determine closed loop conditions § However, certain results may be obtained directly For example, note that for $C = 1$, $K = 0$ is a solution of $Z_{(x_2)} = 0$ for any Ω On the other hand, for large K, series expansion of the terms in Eq (21) results in the condition

$$C \rightarrow [(2\Omega + 1)/3]^{1/2} \qquad (37)$$

in the limit $K \rightarrow \infty$ These two points will be useful in interpreting the behavior of the closed loop conditions for various values of Ω

These classifications are summarized graphically in Fig 5, in which the domains of each type curve are indicated on a plot of K vs C with Ω as the parameter The curves for $\Omega = 0$ are identical to those of Ref 3 The effects just discussed

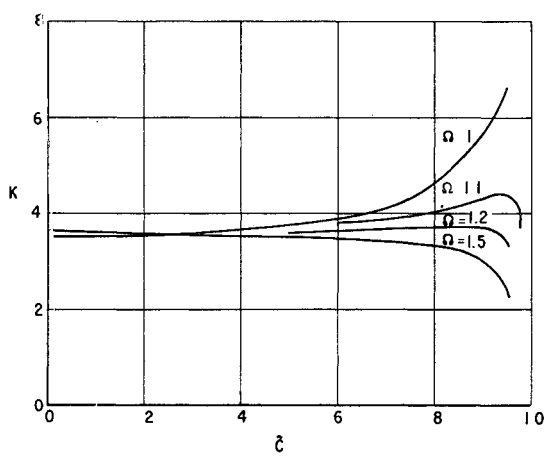

Fig 6 Closed loop conditions for $\Omega = 1$

§ For $\Omega = 0$, it is possible to express all parameters in terms of the modulus of the elliptic integrals as the only unknown, greatly reducing the labor in calculating closed loop conditions

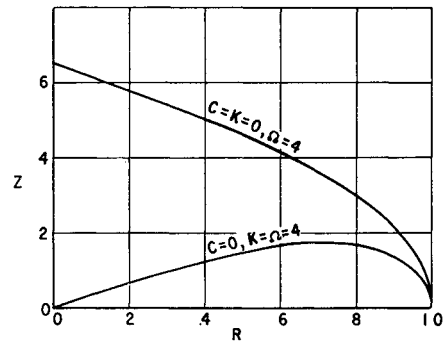

Fig 7 Sample meridian curves, $C = 0$

are evident in the graph Thus, cylinders are possible for $0 \leq \Omega \leq 1$, whereas cusps are possible for all values of $\Omega \geq 0$

The character of the closed loop boundary is drastically different for $\Omega \leq 1$ than for $\Omega > 1$ For $\Omega \leq 1$, the closed loop condition requires $K \rightarrow \infty$ for some $C \leq 1$, in accordance with Eq (37) For $\Omega > 1$, however, this asymptote no longer exists ($C > 1$) and the condition $K = 0$ at $C = 1$ for all Ω now dominates the behavior of the closed loop boundary for C near unity In Fig 6, the closed loop boundaries are shown for $\Omega = 1$, 1 1, 1 2, and 1 5, clearly demonstrating this behavior

B Sample Results

Meridian curves are plotted in Figs 7 and 8 for the following cases:

Case 1

$$C = 0 \qquad K = \Omega = 4$$

Case 2

$$C = 0 \qquad K = 0, \Omega = 4$$

Case 3

$$C = 0\,5 \qquad K = \Omega = 4$$

Case 4

$$C = 0\,5 \qquad K = 0, \Omega = 4$$

The value $\Omega = 4$ was chosen for convenience In particular, the value $Z_{(0)} = 0$ results for case 1 Figure 7 shows the effect of pressure on a centrifugal loaded filamentary structure In general, a more convex shape results, as expected Note that the two curves of Fig 7 are not the same structure since the filament length is different for the two cases By scaling to the same filament length, the equatorial radius would be different for the pressurized vs unpressurized structure Figure 8 shows the same effect when the filament is not meridian wrapped The general shape of the meridian curve is the same as for $C = 0$ except in the vicinity of the axis A central hole must exist for any helix-wound fila-

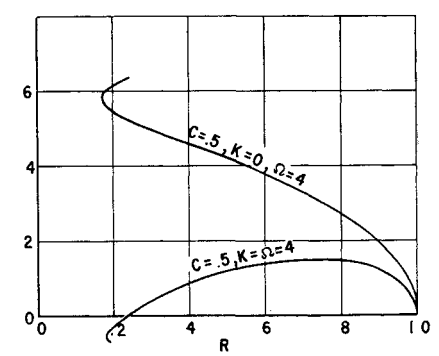

Fig 8 Sample meridian curves, $C = 0\,5$

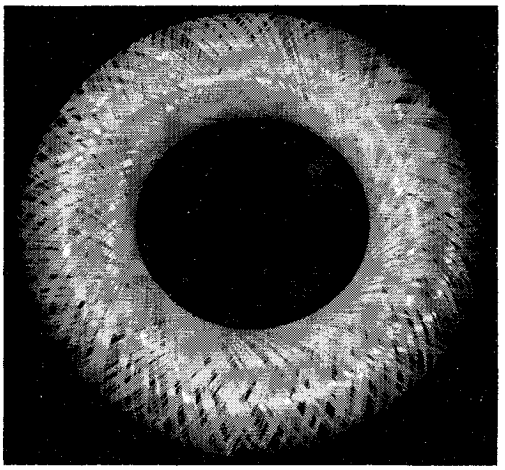

Fig 9 Closed loop toroid pressure vessel, $C = 0\ 35$, $K = 4\ 4$

mentary structure since the filaments cannot intersect the axis of rotation (except for $C = 0$) Note that in Fig 8 the curve for $K = 0$ is a corrugated tube, and the curve for $K = 4$ is a regressive loop, as indicated by the domains in Fig 5

V Experiment

For the purpose of realizing the predicted equilibrium shapes of rotationally symmetrical filamentary structures, two types of experiments were conducted

First, a series of pressure vessels were made by filament winding processes from a reasonably flexible material For the purpose of experimentation, the toroidal type of pressure vessel was selected This choice was made in view of the inherent simplicity, high performance potential, and general interest for practical applications of toroidal pressure vessels

By applying design internal pressure the shell geometry was stabilized, and the equilibrium contour was recorded and compared to the analytically predicted shapes By further raising the internal pressure to the burst point, various mechanisms of failure could be observed and interpreted in terms of materials properties and structural stability characteristics

Secondly, a single, heavy filament in the form of a link chain was subjected to centrifugal forces Its geometrical arrangement was recorded and compared to analytically derived data

A Pressure-Vessel Tests

Several toroidal pressure vessels were designed and fabricated, using a high-rigidity polyester fiber (Dacron) in com-

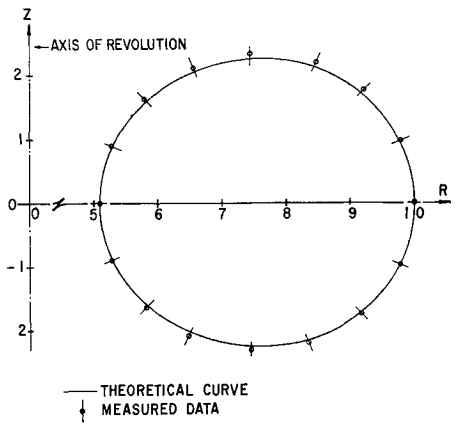

Fig 10 Theoretical vs experimental contour geometry of closed loop toroid pressure vessel

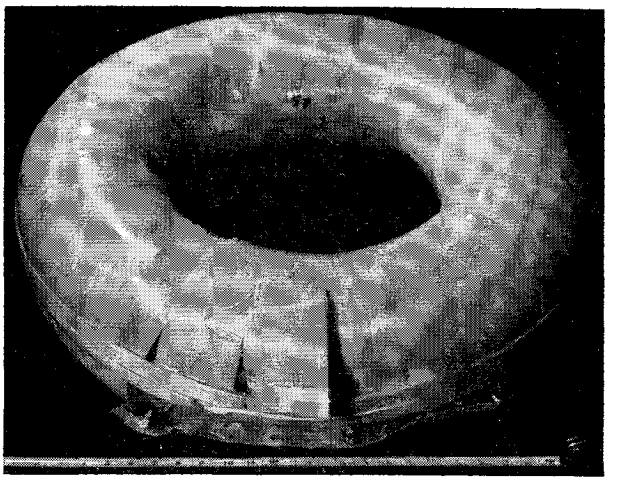

Fig 11 Toroid pressure vessel—failure by exceeding filament strength

bination with elastomeric matrix and liner materials A typical "closed loop" vessel, in a stage of partial completion, is shown in Fig 9 The design parameters for this structure are $C = 0\ 35$, $K = 4\ 4$, $\Omega = 0$ The degree of agreement between measured and analytically predicted cross-sectional contour is shown in Fig 10

Similar tests were conducted with pressure vessels employing combinations $C = 0$ (meridional windings) and $C = 1$ (equatorial windings) Figure 11 shows a typical strength failure resulting from exceeding the basic materials strength in the $C = 0$ portion of the pattern Figure 12 shows a typical hydrostatic stability failure of a similar pressure vessel designed to exhibit this phenomenon An analysis of one type of hydrostatic instability pertinent to this type of failure is presented in Sec VI

B Tests on Rotating Structures

For the purpose of realizing the analytically predicted geometry of a rotating filament, the simple case of $K = 0$, $\Omega = 4$, and $C = 0\ 5$ was chosen

Nondimensional ordinate Z, arc length L, and central angle φ were computed for the abscissa $R = 0\ 4$ from Eqs (22, 33, and 28c), respectively, yielding $Z = 0\ 46$, $L = 0\ 87$, and $\varphi = 29°$ To generate the corresponding geometry, a metal chain of appropriate length was supported on two disks with the attachment points rotated and spaced relative to each other by the indicated central angle and distance The disks, in turn, were supported by a quill mounted into the spindle of a modified lathe, equipped with a variable speed drive The test equipment with rotating chain is shown in a time exposure photograph by Fig 13 A flash exposure photograph of the same setup, revealing the instantaneous geometry assumed by the chain, is shown in Fig 14

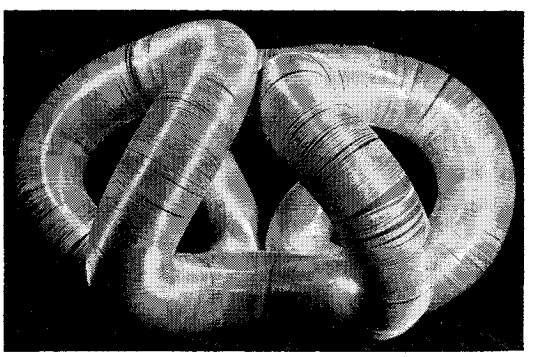

Fig 12 Toroid pressure vessel—typical hydrostatic instability failure

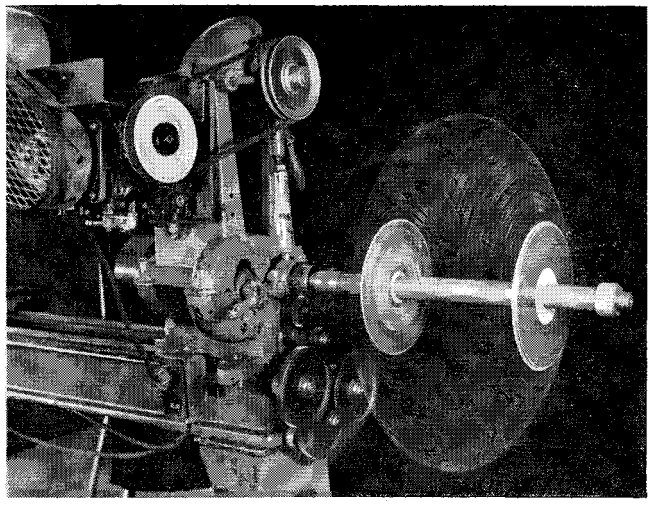

Fig 13 Rotating chain geometry—time exposure

The geometry of the rotating chain was recorded by photography, using both flash and time exposure to obtain end view, side view, and envelope contour of the rotating chain For this purpose, the quill assembly was removed from the fixture after the first exposure of the rotating chain on a tripod-mounted Polaroid camera An inked reference grid was then placed into the appropriate normal or axial center plane of the body of revolution generated by the revolving chain to minimize parallax errors The camera shutter was then tripped for the second exposure of the film

A theoretical computation was made for the end view, side view, and envelope contour (meridional shape) for the selected parameter triplet The results of this computation, together with experimental data points obtained from the photographic records, are shown in Fig 15 The experimentally obtained data were found to agree with the theoretically predicted geometrical shapes within reading accuracy of the photographic records

VI Application

Applications for the analytical techniques presented in this report fall into two broad categories: the design synthesis of optimized filamentary structures in which the structural properties of the filaments are utilized to the fullest possible extent, and the study of specific problems arising in the structural analysis of filamentary structures The latter application is of particular interest in the case of large elastic deformations observed in pressure-stabilized structures subject to external loads, and in the study of the static stability of such structures

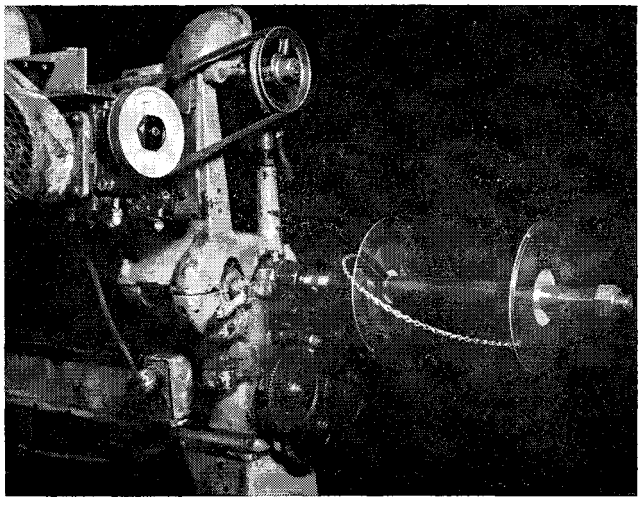

Fig 14 Rotating chain, flash exposure

In the treatment of these problems of analysis, the assumption may be made that the filaments remain inextensional and completely compliant in bending and that the matrix or liner material remains stress-free during the deformation With these assumptions, a point of departure for analysis is found in the intrinsic properties of the filamentary structure, i e , in the properties which will not change during the deformation process Such intrinsic properties are either topological or metric in nature

Retention of intrinsic topological properties as they apply to the over-all structural configuration will form, in general, the end points or constraints of possible deformation (i e , a toroid will remain in a toroid throughout the deformation) Intrinsic topological properties, as they apply to the filamentary geometry, are of somewhat more subtle character and involve, for instance, the number of turns of the filament around the structure and the periodicity of the turns per revolution This characteristic is particularly evident in the case of the smooth toroid where the number of filament turns around the toroid necessary to complete a full revolution of the central angle φ in the winding pattern constitutes an intrinsic property of the filamentary structure

Intrinsic metric properties are, according to the assumptions of inextensional fibers just stated, the lengths of the filaments Additional intrinsic metric properties may be stated for specific problems, such as a condition that crossover points of differently oriented filament systems may not slide with respect to each other (trellis-condition)

The problem of structural analysis of a given filamentary structure, subject, for instance, to an external load, thus reduces to finding related structural configurations with appropriately identical intrinsic properties and with the required discontinuities at the locations of load application

For the purpose of illustration, two examples for this type of analysis are summarized here The first example considers a structural element consisting of a nonrotating ($\Omega = 0$) bottle-shaped pressure vessel with meridional windings ($C = 0$) anchored at two circumferential rings ($C = 1$)

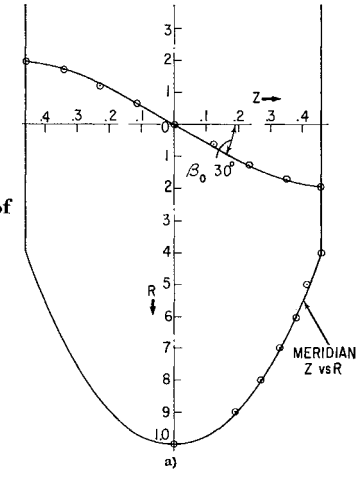

Fig 15a Side view of chain $R \sin\varphi$ vs Z

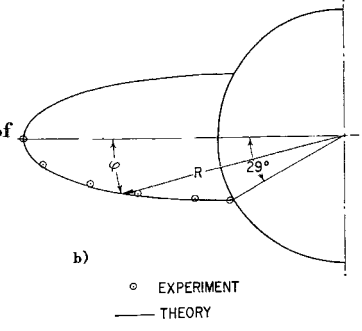

Fig 15b End view of chain R vs φ

as shown in the inset of Fig 16 This element can be considered as either representing the structural portion of a spheroidal rocket motor case, or can be considered as an element of a "corrugated" structural column

Consider now this structure subject to an axial load P The deformed configuration will retain the length of the filament between the rings and the circumferential length of the rings Since the nature of the deformation is such that axisymmetry is retained, the possible shapes of deformation can be established by holding the filament length of the meridian and the radius of the rings invariant, for a range of selected K values, which in this case are conveniently normalized for the invariant ring radius Results of this procedure, in terms of normalized load-deformation characteristics, and for an arbitrarily assumed constant internal pressure, are shown in Fig 16, indicating the expected nonlinear elastic behavior of the structure similar to that studied in detail in Ref 8

The second example considers a range of nonrotating pressurized toroids formed by two branches of a meridional winding pattern joining an outer and inner equatorial ring, as shown in the inset of Fig 17 The toroids are designed for parameter values of $K = 5$, $C = 0$, and $\Omega = 0$ in a condition without externally applied loads A range of designs is generated by varying the intercept location of the two

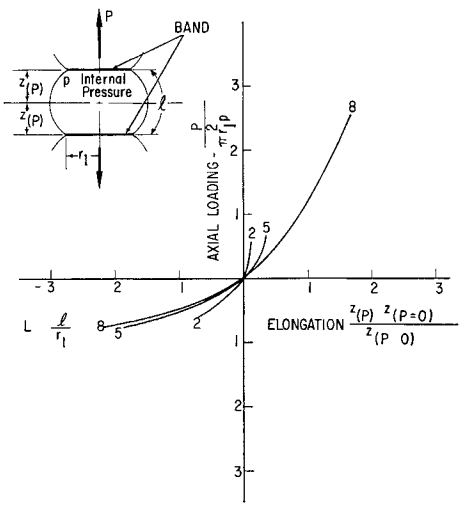

Fig 16 Load-deformation characteristics of pressure stabilized, corrugated cylinder

branches or, in other terms, the radii r_1 and r_2 of the outer and inner equatorial rings These radii are related to the ring cross sections (or number of filament turns n_1 and n_2) by the condition that the stress level in the fibers forming the equatorial bands be equal to the stress level in the fibers forming the meridional winding pattern (isotensoid condition)

An axisymmetrically distributed and axial loading P is considered, acting at the outer ring and reacted by an equal and opposite load applied at the inner ring The question considered here is that of initial spring rate (i e , the stiffness for small deformations from the unloaded equilibrium configuration) as it is affected by the particular choice of the ring radii and related number of turns in the rings The results of this investigation, based upon intrinsically invariant filament length and the assumption of invariant internal pressure, are shown in Fig 17 It will be observed that there exists a critical parameter configuration at which the spring rate vanishes, indicative of a state of marginal static stability of the structure For negative spring rates, a statically unstable structure can be identified, exhibiting a "geometrical" instability in the sense that only geometrical and no material properties enter into the mechanism causing instability

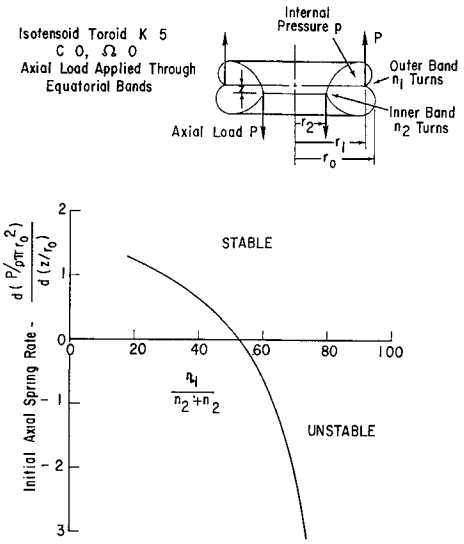

Fig 17 Initial spring-rate of axially loaded isotensoid toroids in function of design parameter $n_1/(n_1 + n_2)$

VII Concluding Remarks

The filamentary structures considered in this report represent idealizations of actual structures in several respects and the importance of each will need to be assessed in specific applications in view of the individual case The idealizations selected were such that relatively straightforward analytical formulation for the pertinent geometrical characteristics of the filamentary structures considered could be developed These prove useful for gaining insight into the general nature of the problems in design and operation of such structures

In addition, the basic differential equations presented lend themselves to considerable generalization including the case of nonuniform internal pressure (of practical importance for rocket motors subject to distributed inertia loads and for the design of inserts and end-closure attachments) These problems can be readily solved by digital integration, such as those presented previously [3] The value of the analytical formulations in this case is that of allowing a check for the computor programs by testing them on an idealized case for which the result can be readily verified analytically as well as by providing means of initializing the digital programs

Idealizations that may be serious limitations in specific applications rest in the basic concept of monotropic membrane arrays as representative for the structure Where matrix materials of significant stiffness are used, the assumption that matrix materials will not contribute to the primary stress system must be questioned Also inherent in the concept of monotropic membranes is the assumption of negligible wall thickness For the case of thick-walled pressure vessels, specifically in areas of polar buildup due to cross-over of the winding pattern, a refined method somewhat reminiscent of a "stress concentration" analysis might be developed

Finally, the case of deviations from axisymmetry remains to be studied from two points of view: the structure originally may be built with operationally required deviations from axisymmetry (as, for instance, in the case of multiple nozzle and retroports in filament-wound solid propellant rocket motors); or, nonaxisymmetric loading on originally axisymmetric structures may cause deviations in the deformed state A general approach to such problems, using the technique of differential geometry, has been outlined, but not implemented, in Ref 3 The mathematical difficulties, at first sight, appear formidable Digital techniques, although cumbersome, may be developed to effectively solve critical problems in this area in the future

Appendix: Weight and Performance of Optimum Pressure Vessels

The structural performance of a pure pressure vessel ($\Omega = 0$) may be expressed in terms of the weight required to enclose a given volume at a given working pressure

The following general energy considerations show that, unlike the pressure vessels made from isotropic materials such as sheet metals, the structural performance of filament-wound pressure vessels is independent of shape, provided that they meet the conditions of optimum isotensoid design

The mechanical work (PE) done by internal pressure p in expanding the shell equals one-half the pressure times the volumetric expansion ΔV For small, uniform linear strains in the container wall, the volumetric expansion equals $3\epsilon V$, where V is the total container volume Thus,

$$\Delta V = V(1 + \epsilon)^3 - V = 3\epsilon V + \text{terms of smaller order} \tag{A1}$$

and

$$(PE) = p\Delta V/2 = 3\epsilon Vp/2 \tag{A2}$$

This work is stored in the form of strain energy in the structure For an ideal filamentary material, the only stress possible is the unidirectional stress f Furthermore, stresses and strains are, by definition, uniform Thus, the strain energy (SE) stored in a structure of weight W and density ρ can be written as

$$(SE) = \epsilon f(W/\rho)/2$$

Introducing a specific materials strength $s = F_{tu}/\rho$, where F_{tu} is the unidirectional ultimate tensile stress and a safety factor $(SF) = F_{tu}/f$, it is seen that the expression for strain energy can be transformed to

$$(SE) = \tfrac{1}{2}\epsilon W(f/\rho) = \tfrac{1}{2}[\epsilon s/(SF)]W \tag{A3}$$

Equating the work done by internal pressure to the strain energy stored in the container structure yields

$$3Vp = W[s/(SF)] \tag{A4}$$

or

$$W = 3V(p_{ult}/s) \tag{A5}$$

where $p_{ult} = p\ (SF)$ is the conventionally-defined ultimate burst pressure

Thus, it may be seen that the structural weight required to enclose a given volume at a given pressure depends solely upon the specific materials strength s and is independent of the particular shape of the isotensoid pressure vessel

In comparing the theoretical weight-volume-pressure relation expressed by Eq (A5) with results obtained in current designs, a design efficiency factor η can be used The actual weight of the load-carrying structure can be expressed in terms of the theoretical isotensoid weight as follows:

$$W_{total} = W' + 3(Vp_{ult}/\eta s) \tag{A6}$$

where W' denotes the "parsitic" weight associated with pressure liners, brackets, etc From Eq (A6) it can be seen that the design efficiency η is the fraction of the basic materials strength available as "actual" or "design" strength in the filament-wound structure The design efficiency is, therefore, an indicator for the quality and maturity of the design; it is a measure of the ability of the design to exploit the full potential strength of the basic material

A review of filament-wound pressure vessels currently produced for rocket motor cases[10] indicates that typical values obtained for design efficiency in this field are in the neighborhood of 50–60% Prototype isotensoid toroids, on the other hand, typically have produced values for design efficiency of about 90%

In an assessment of the relative merits of different design approaches to the same end objective, care must be taken that all contenders are compared on a basis of equal design maturity and design sophistication For the case of a pressure vessel, it is possible to define optimum design configurations for either filament-wound or sheet-metal construction, and the relative merits of the two approaches can be compared, for instance, in terms of the structural weight required to enclose a given volume at a given internal pressure

For a sheet-metal pressure vessel (i e , a thin-walled pressurized structure made from an isotropic material), the

Table 2 Properties of pressure vessel materials

	t_m, melting point, °F	ρ, density, lb/in^3	E, modulus 10^6 in	E/ρ, 10^6 in	F_{tu}, Ult str , 10^3 psi	$S = F_{tu}/\rho$, Sp str , 10^6 in
Sheet metal						
Al alloy	1680	0 10	10	100	75	0 75
Steel	2700	0 29	29	100	290	1 0
Beryllium	2790	0 067	40	600	80	1 2
Titanium	3500	0 16	16	100	195	1 2
Filaments						
Dacron[e]	450[a]	0 050	1 9	38	140	2 8
E-glass	1400[a]	0 09	9	100	300	3 3
X-994-glass	1400[a]	0 09	10	110	400	4 4
Carbon steel wire	2700	0 29	29	100	640	2 2
Boron filament	3700	0 09	55	610	500[d]	5 5
Tungsten filament	6170	0 70	50	71	600	0 9
Pyro graphite	>6000[b]	0 08	4	50	50[d]	0 6
80% Fiber—20% matrix composites						
Dacron-polyurethane	400[a]	0 05	1 5	30	112	2 2
E-glass epoxy	450[a]	0 082	7 2	87	240	2 9
X-994 glass-epoxy	450[a]	0 082	8 0	98	320	3 9
Steel wire polyurethane	450[a]	0 24	23	96	510	2 1
Boron-epoxy	450[a]	0 082	45	550	400[d]	4 9
Tungsten-carbon	4300[c]	0 58	40	69	480	0 8
Pyrographite-carbon	>6000[b]	0 08	3 6	45	40[d]	0 5

[a] Softening or decomposition temperature
[b] Sublimation temperature
[c] Limited by carbide formation
[d] Preliminary data
[e] Heat stretched material

optimum geometry is the sphere For a given burst pressure p_{ult} and enclosed volume V, the weight of a spherical pressure vessel can be expressed as

$$W_{sm} = 1\,5\,\frac{V_{p_{ult}}\rho_{sm}}{F_{tub}\eta_{m}} + W_{m}' \qquad \text{(A7)}$$

where W_{sm}' denotes parasitic weight contributions from valves, openings, reinforcements, weld beads, etc ; ρ_{sm} denotes density; F_{tub} is the ultimate tensile stress of the material under conditions of uniform biaxial stress; and η_{sm} is the design efficiency

For the filament-wound construction, the optimum configuration is the isotensoid involving a wide range of shapes including spheroids, toroids, and cylinders The basic structural weight associated with the isotensoid is independent of the particular configuration chosen and may be expressed in a manner similar to that used for the sheet metal design,

$$W_{fw} = 3\,\frac{V_{p_{ult}}\rho_{c}}{F_{tuu}\eta_{fw}} + W_{fw}' \qquad \text{(A8)}$$

where W_{fw}' again denotes parasitic weights Here F_{tuu} is the ultimate uniaxial stress in the direction of the filament of a uniaxial filamentary layup and referred to the total cross section, and ρ is the average density of the composite material

Expressing the parasitic weight as a fraction f' of the basic structural weight in each case, and introducing the specific strength s for F_{tu}/ρ, we can express the ratio of the total weight for the spherical sheet-metal design to that for any isotensoid filament-wound design as

$$(WR) = \frac{W_{sm}}{W_{fw}} = \frac{s_{fw}}{2s_{sm}}\,\frac{1+f'_{sm}}{1+f'_{fw}}\,\frac{\eta_{fw}}{\eta_{sm}} \qquad \text{(A9)}$$

This expression shows that the relative weight ratio (WR) depends on three factors: the ratio of the obtainable specific strengths of the materials, a parasitic weight factor, and the ratio of design maturity of the two approaches Typical physical and mechanical materials properties for conventional and advanced pressure vessel materials are are listed in Table 2 The parasitic weight factor needs to be assessed in view of the particular design that is envisioned The design maturity factor should be taken as unity if a fair comparison of the two approaches is to be made

For the purpose of such a comparison, consider a pressure container for an ultimate pressure of 10,000 psi and an enclosed volume of 3460 in ^{3} (2 ft^3) The highest performance in sheet-metal design can be obtained with titanium With a parasitic weight factor of $f_m = 0\,02$ and a design efficiency of 100% an optimum spherical welded titanium pressure vessel would weigh

$$W_{sm} = \frac{1\,5 \times 3460 \times 10{,}000}{1\,2 \times 10^6}\,(1\,02) = 44\,1 \text{ lb}$$

A toroidal container made from high-quality glass fiber-epoxy composite (X-994 glass) would have a parasitic weight fraction associated with valves, liner, etc , of 0 08 For this pressure vessel the weight would be

$$W_{fw_{(glass)}} = \frac{3 \times 3460 \times 10{,}000}{3\,9 \times 10^6}\,(1\,08) = 28\,8 \text{ lb}$$

which represents a reduction in weight of 34% compared to the best welded titanium construction It should be noted that this gain in performance is also associated with a potentially considerably lower cost for the finished product, as compared to welded titanium construction

Where cost of materials is no object, a boron-filament-wound toroidal container can be considered If an equal parasitic weight fraction is assumed, the total weight would be

$$W_{fw_{(boron)}} = \frac{3 \times 3460 \times 10{,}000}{4\,9 \times 10^6}\,(1\,08) = 22\,9 \text{ lb}$$

which provides a weight reduction of 47% compared to the best competitive sheet-metal design

References

[1] Green, A E and Adkins, T E , *Large Elastic Deformations and Non-Linear Continuum Mechanics* (Oxford University Press, Oxford, England, 1960), Chap VII

[2] Harmon, R F S , "The elastic constants of anisotropic materials" Rev Mod Phys **18**, 429 (1946)

[3] Schuerch, H U , Burggraf, O R , and Kyser, A C , "A theory and applications of filamentary structures—Part I: Theoretical studies," Rept ARC-R-30, Astro Research Corp (September 1961)

[4] Hoffman, G A , "The effect of filamentary materials on pressure vessel design," *Proceedings of International Astronautical Congress* (Pergamon Press, New York, 1960)

[5] Schuerch, H U , "Space structure design with composite materials," ARS Preprint 1096-60 (April 1960)

[6] Zickel, J , "Isotensoid pressure vessels," ARS J **32**, 950–591 (1962)

[7] Byrd, P F and Friedman, M D , *Handbook of Elliptic Integrals for Engineers and Physicists* (Julius Springer-Verlag, Berlin, 1954)

[8] Kyser, A C , "A contribution to the theory of large deformations in pressure stabilized structures," Astro Research Corp , ARC-R-75 (Septenber 1962)

[9] Selfridge, R G and Maxfield, J E , *A Table of the Incomplete Elliptic Integral of the Third Kind* (Dover Publications Inc New York, 1958)

[10] Bert, C W and Hyler, W S , ' Design considerations in selecting materials for large solid-propellant rocket motor cases," DMIC Rept 180, Defense Metals Information Center, Battelle Memorial Institute (December 1962)

[11] Hartung R F "Membrane analysis of orthotropic filament wound pressure vessels," Lockheed TR 3-80-62-1 (February 1962)

[12] Isotensoid structures, U S Patent No 312 1451, issued to Astro Research Corp (February 18, 1964)

[13] Nourse, J H , "The ovaloid problem A definition and geodesic ovaloid solution," Glass Filament Research and Development Symposium, Lockheed Missiles and Space Company (July 1961)